Environmental Science & Technology

pubs.acs.org/est

Article

Dissolved Organic Matter Composition Determines Its Susceptibility to Complete and Partial Photooxidation within Lakes

Reid P. Milstead, Emma R. Horvath, and Christina K. Remucal*

Cite This: *Environ. Sci. Technol.* 2023, 57, 11876−11885

Read Online

ACCESS | Metrics & More | Article Recommendations | Supporting Information

ABSTRACT: Dissolved organic matter (DOM) plays an important role in carbon cycling within inland surface waters. Under sunlight irradiation, DOM undergoes complete photooxidation to produce carbon dioxide (CO_2) and partial photooxidation that alters the molecular composition of DOM. However, a mechanistic understanding of the relationship between DOM composition and its susceptibility to partial and complete photooxidation in surface waters is currently lacking. This work combines light exposure experiments with high-resolution mass spectrometry to investigate DOM photooxidation using two DOM isolates and DOM from 16 lakes that vary in trophic status and size. High ratios of oxygen consumption to dissolved inorganic carbon (DIC) production demonstrate that all samples undergo extensive partial photooxidation. At the molecular level, more oxidized, aromatic DOM formulas are associated with oxygen consumption and DIC production. Bulk level measurements indicate that DOM becomes less aromatic and lower in apparent molecular weight following partial photooxidation, and there is molecular level evidence of oxygen addition and loss of CO_2 in all samples. However, formulas most susceptible to photooxidation vary depending on the initial DOM composition. Collectively, this work provides insights into the relationship between DOM composition and photooxidation, which has important implications for carbon cycling in diverse surface waters.

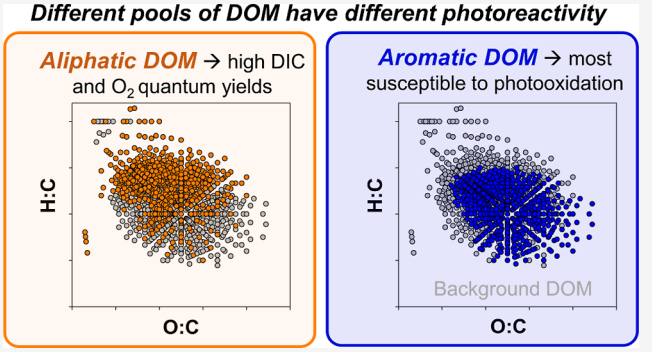

KEYWORDS: *high-resolution mass spectrometry, photochemistry, carbon cycling, organic carbon, water*

Downloaded via UNIV OF WISCONSIN-MADISON on February 27, 2024 at 19:36:58 (UTC).
See https://pubs.acs.org/sharingguidelines for options on how to legitimately share published articles.

INTRODUCTION

Inland surface waters, such as lakes, play an important role in the global carbon cycle despite making up <1% of the Earth's surface area.[1] Lakes and their sediments are major carbon pools and contribute to storage, transport, and processing of organic carbon.[1,2] For example, the processing of dissolved organic matter (DOM) can mineralize organic carbon and produce carbon dioxide (CO_2), an important greenhouse gas.[3,4] As a result, lakes are typically net sources of CO_2 to the atmosphere.[2,5] For example, lakes in the Northern Highlands Lake District in Wisconsin, USA release 28 Gg-C/yr, which is ∼14% of local CO_2 emissions.[2] On a global scale, lakes and inland surface waters release 2.1 Pg-C/yr,[6] which is equivalent to ∼6% of global carbon emissions from fossil fuel use in 2020 (34.8 Pg-C/yr).[7] Thus, lakes are hotspots of carbon cycling and greenhouse gas emissions. It is important to understand how organic carbon is processed in these environments to create accurate carbon budgets.

DOM transformation within lakes occurs via either biological processing or photolysis. Both mechanisms can result in partial oxidation that alters the composition of DOM or complete oxidation (i.e., mineralization) to CO_2.[8] Microbial processing is often considered to be more important than photolysis in surface waters.[4,9] However, several studies suggest that photooxidation may be dominant in certain environments, particularly in terms of CO_2 emissions.[4,9] The relative importance of each pathway likely depends in part on the composition of DOM. For example, photooxidation may be responsible for ∼10% of DOM mineralization (i.e., complete photooxidation) in Swedish lakes[10] and up to 33% of CO_2 production in terrestrially dominated arctic lakes on a landscape scale.[4] Despite the potential importance of photooxidation for DOM processing, lake carbon cycling models generally do not include photooxidation or consider variable DOM composition in these systems.[2,3,11]

In addition to complete oxidation, DOM composition can be altered by partial oxidation. Partial photooxidation, which is characterized by high ratios of oxygen (O_2) consumption to CO_2 production,[8,12,13] can be dominant over microbial partial

Received: February 23, 2023
Revised: July 10, 2023
Accepted: July 17, 2023
Published: July 31, 2023

ACS Publications

© 2023 American Chemical Society

oxidation in some environments.[4] Changes in DOM composition have implications for its subsequent reactivity. For example, photooxidation of DOM can produce small acids, such as carboxylic and pyruvic acids,[14−17] that are readily bioavailable. Alternatively, photooxidation can form more recalcitrant DOM, such as carboxyl-rich alicyclic molecules.[18,19] As a result, photooxidation has been shown to either increase[14,16,20,21] or decrease bioavailability of DOM,[18,19] with several studies observing both trends.[22−28] Previous studies using bulk scale analyses such as ultraviolet−visible (UV−vis) and fluorescence spectroscopy[9,29−33] and size exclusion chromatography[33] demonstrate that aromaticity[29−31] and molecular weight (MW) typically decrease during photolysis.[9,30,33−35] Analysis by high-resolution mass spectrometry generally show similar removal of aromatic formulas[9,32,36,37] and formation of more saturated photoproducts.[9,12,22,32,34,36−38] However, changes in extent of oxidation are variable, with both increases[38] and decreases[32] reported. Existing studies using both bulk and high-resolution analyses are limited to a few samples or locations in a single study, making it difficult to explain variable trends across different waters.

The aim of this study is to investigate how DOM composition impacts its susceptibility to partial and complete photooxidation. We characterize DOM using bulk measurements and high-resolution mass spectrometry before and after photooxidation to fully assess changes in DOM composition. These data are then combined with O_2 consumption and inorganic carbon production measurements to develop the first molecular level relationships for photomineralization, building on previous attempts to relate bulk level DOM composition to its photoreactivity.[9,18,22,39] We use the North Temperate Lakes-Long Term Ecological Research (NTL-LTER) network to obtain samples with highly variable DOM composition, as well as nearshore sites on Lake Michigan and Lake Superior, potentially making the results of this study applicable to a wide range of surface waters.

MATERIALS AND METHODS

Sample Collection and Materials. Samples were collected in May 2021 from lakes in the NTL-LTER network[40] in the Northern Highland Lakes District and the Yahara watershed in Wisconsin, USA. Northern lakes include Trout Lake (O4), Trout Bog (D2), Sparkling Lake (O3), Crystal Bog (D1), Crystal Lake (O2), Allequash Lake (M1), and Big Muskellunge Lake (O1). Yahara watershed lakes include Lakes Mendota (E1), Monona (E2), and Wingra (E3). Samples were collected just under the surface at designated buoys in each lake (Tables S1 and S2). Three samples each were collected from nearshore Lake Michigan (G1−G3) and Lake Superior (G4−G6; depth <30 cm). Samples were filtered through 0.45 μm glass fiber filters within 48 h of collection and stored in pre-baked (450 °C, 8 h) amber glass jars at 4 °C in the dark; samples were re-filtered every 6 months and before all experiments. Organic matter isolates Suwanee River NOM (I1) and Upper Mississippi River NOM (I2) were used to enable comparison with other studies. All chemicals are described in Section S2.

Bulk Water Chemistry. Sample pH was measured using a Mettler Toledo EL20 meter. Dissolved organic carbon ([DOC]) and dissolved inorganic carbon ([DIC]) concentrations were measured using a GE Sievers M5310C total organic carbon analyzer. Ions and metals were quantified using ion chromatography (Table S3) and inductively coupled plasma optical emission spectroscopy (Table S4), respectively.

UV−vis spectra were collected using a Shimadzu 2401PC spectrophotometer in 1 nm increments from 200 to 800 nm and referenced against ultrapure water. Specific UV absorbance ($SUVA_{254}$) was determined by dividing absorbance at 254 nm by [DOC].[41] E_2:E_3 is the ratio of absorbance at 250 to 365 nm.[29] Electron donating capacity (EDC) was determined using a spectrophotometric method (Section S3).[42−44] Fluorescence excitation emission matrices were collected using an Horiba Aqualog in 5 nm excitation increments from 250 to 800 nm, referenced against ultrapure water, and corrected for inner filter effects and Rayleigh scattering. Fluorescence index (FI), humification index (HIX), and biological index (BIX) were determined as described in Section S3.[45−47]

Dissolved Gas Quantification. Dissolved oxygen consumption and inorganic carbon production were quantified in 17 mL glass TOC vials, which were filled with air-saturated samples with no headspace and closed with screw top septa caps. DIC production was used as a proxy for CO_2 production. Caps were wrapped in parafilm to further limit gas exchange (Figure S1). Samples were irradiated in triplicate in a Rayonet photoreactor with 365 ± 10 nm bulbs.[48] These wavelengths are within the solar spectrum, overlap with DOM absorbance spectra, and are important for DOM photomineralization.[4,37,49−51] Dark controls remained at 23.9 ± 0.2 °C, while light-exposed samples reached 26.9 ± 0.1 °C. Samples were irradiated for 22 h based on preliminary kinetics experiments (Figures S1, S2, and Section S4).

Due to their high ambient [DIC] (Table S1), Yahara watershed samples were adjusted to a pH of 2.5, sparged with nitrogen gas for ≥30 min to remove DIC, and readjusted to the original pH prior to dissolved gas irradiation experiments as described previously.[10] pH adjustment and sparging remove some organic compounds and may impact apparent quantum yield values.[52] Organic matter isolates (5 mg-C/L) were prepared using air-saturated ultrapure water and adjusted to a pH of 7.5 using sodium hydroxide but were not buffered. All other experiments were conducted using waters with ambient [DIC]. pH stayed within ±0.5 units during photolysis. All experiments were conducted in triplicate alongside a *para*-nitroanisole/pyridine actinometer.[53,54] Identical triplicate sample vials were held at room temperature in the dark as controls. Inorganic carbon concentrations (i.e., the sum of CO_2, carbonic acid, bicarbonate, and carbonate) were quantified in acidified samples using a total organic carbon analyzer (LOD = 0.68 μM DIC). Dissolved oxygen was quantified using a FireSting-GO2 oxygen meter (PS-FSGO2) and an oxygen probe (PS-OXROB10; LOD = 4.69 μM). $SUVA_{254}$, E_2:E_3, EDC, and fluorescence indices were quantified in irradiated samples as described above.

Quantum Yields. The actinometer was used to calculate light intensity as described previously.[54] Quantum yields of DIC production (Φ_{DIC}) and oxygen consumption (Φ_{O2}) were calculated as described in Section S5.

High-Resolution Mass Spectrometry. Irradiation experiments to assess changes in DOM molecular composition relative to dark controls were conducted in 500 mL samples in borosilicate glass bottles. The larger volume was used to facilitate solid-phase extraction (SPE). All samples were irradiated for 24 h, which resulted in the same photon flux as that observed over 22 h in smaller containers (Figure S3). In addition, six samples (M1, D2, E1, O1, G3, and I1) were

https://doi.org/10.1021/acs.est.3c01500
Environ. Sci. Technol. 2023, 57, 11876−11885

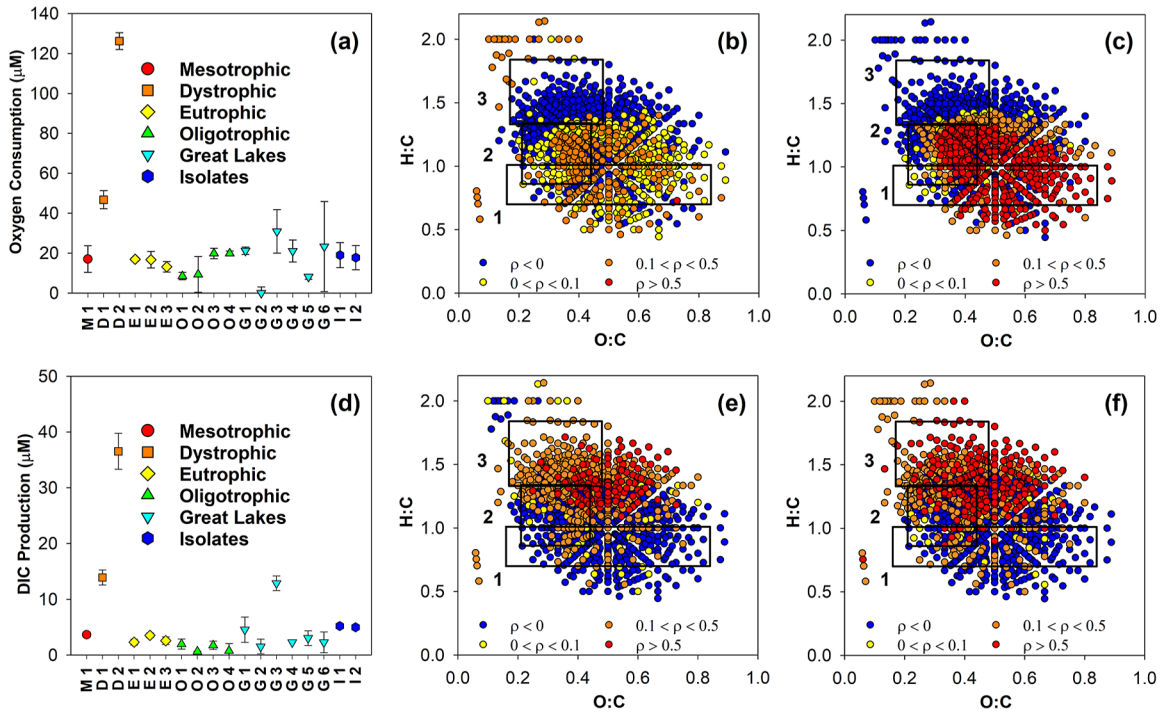

Figure 1. (a) DOC and (d) DIC (i.e., a proxy for CO_2) production following 22 h of photoirradiation. Spearman rank correlations between the relative intensity of common DOM formulas and (b) carbon-normalized oxygen consumption, (c) carbon-normalized DIC production, (e) Φ_{O2}, and (f) Φ_{DIC}. Formulas that are positively correlated with these parameters are in yellow, orange, and red. Negative correlations are in blue. Formulas were found in all 14 samples with detectable changes in gas concentrations. Boxes correspond to (1) lignin-, (2) tannin-, and (3) protein-like regions.[79]

irradiated for 2, 6, and 24 h to assess the kinetics of DOM composition changes in samples with varying changes in dissolved gas concentrations.

DOM was extracted from samples before and after light exposure using SPE.[55−58] Samples (500 mL) were acidified with hydrochloric acid (pH < 2.0) and loaded onto activated (5 mL methanol) BondElut PPL cartridges. The cartridges were rinsed with 0.1% HCl (1 mL), opened to achieve dry sorbent beds, and extracted with methanol (5 mL). Previous studies using this SPE method report extraction efficiencies of ∼60%.[55,59,60]

Methanol extracts were diluted 100x in 60:40 acetonitrile/H_2O and analyzed using Fourier transform ion cyclotron resonance mass spectrometry (FT-ICR MS; SolariX XR 12T) via direct injection with negative mode electrospray ionization (voltage = −1.4 kV; gas pressure = 0.3 psi; 350 readings per sample). The *m/z* ions with a signal-to-noise ratio of >3 were exported, converted to neutral masses by adding the mass of a proton, and linearly calibrated using common DOM formulas.[54,59−61] Formulas considered for matching included $C_{0\text{-}80}{}^{13}C_{0\text{-}1}H_{0\text{-}140}O_{0\text{-}80}N_{0\text{-}2}S_{0\text{-}1}$. Potential formulas were required to have O:C > 0, 0.3 ≤ H:C ≤ 2.3, and 0 ≤ DBE ≤ 40. Nitrogen-containing formulas were validated using the nitrogen rule. Matched formulas were required to have a <0.5 ppm error and be part of a homologous series (+CH_2 or CH_4 vs O) with at least three members.[62] Weighted averages of elemental ratios (H:C_w; O:C_w) and double bond equivalents (DBE_w) were calculated from identified formulas.[59]

Spearman rank analysis was performed to relate intensities of common matched formulas to dissolved gas concentrations, as well as to DOM parameters (e.g., $SUVA_{254}$). Changes in DOM composition during photolysis were assessed in three ways. First, the time series subset was used to identify changes in formula intensity as a function of irradiation time. Second, changes in formula intensity between initial and final (24 h irradiation) samples were analyzed. Finally, unique photoproduct formulas associated with oxygen addition and loss of CO_2 were identified to determine their mechanism of formation and provide molecular level evidence of partial and complete photooxidation. Additional details are provided in Section S6.

Statistical Analyses. Linear regression analysis was performed on normally distributed data to explore correlations between DOM characteristics, oxygen consumption, and DIC production (Section S6). Error bars represent standard deviation of triplicate measurements.

RESULTS AND DISCUSSION

Variability in DOM Composition. The initial DOM composition is first characterized using bulk scale analyses and high-resolution mass spectrometry. Dystrophic and mesotrophic waters have DOM with high aromaticity ($SUVA_{254}$: 2.5−4.1 L mg-C^{-1} m^{-1}), high apparent MW (E_2:E_3 < 5), high phenolic content (EDC: 1.6−2.1 $mmol_{e^-}$/g-C), and high extent of oxidation (O:C_w ∼0.4; Tables S5−S7). DOM in these waters is similar to terrestrially derived DOM in terms of fluorescence indices (FI ∼1.4, HIX ∼1.0, and BIX <1.0; Table S7)[3,43,45,46,50,59,63−69] and similar to the NOM isolates used in this study. In contrast, DOM from eutrophic and small oligotrophic lakes is less aromatic ($SUVA_{254}$: <2 L mg-C^{-1} m^{-1}), lower in apparent MW (E_2:E_3 > 6), lower in phenolic content (EDC: 0.2−2.5 $mmol_{e^-}$/g-C), and generally more reduced (O:C_w: 0.29−0.45). DOM from these lakes is likely photo-processed and/or microbial in origin (FI >1.5, HIX

https://doi.org/10.1021/acs.est.3c01500
Environ. Sci. Technol. 2023, 57, 11876−11885

<0.8, and BIX >0.7; Table S7 and Figure S5).[46,50] The Great Lakes samples are relatively aromatic ($SUVA_{254}$: 2.0−3.4 L mg-C^{-1} m^{-1}) and have higher apparent MW (E_2:E_3: >5) and low phenolic content (EDC: 0.2−1.6 $mmol_{e^-}$/g-C), which is similar to previous nearshore measurements in Lake Michigan and Lake Superior (Section S7).[61,70−76]

Evidence of Partial Photooxidation. The extent of partial and complete photooxidation is measured by quantifying oxygen consumption and DIC production after irradiation.[4,8] Decreases in oxygen range from <4.7 to 126.5 μM, and increases in DIC range from <0.7 to 36.5 μM. Unlike quantum yields, these absolute gas yields are not corrected for light screening (Table S8). For both gases, values are the highest in dystrophic lakes (D1 and D2) and G3 (Figure 1a,d and Table S8). This trend is partly explained by [DOC] as these three samples have the highest [DOC] (12.0−23.1 mg-C/L vs 2.1−5.5 mg-C/L in all other waters). While oxygen consumption does not have a significant relationship with [DOC], there is a positive relationship between DIC production and [DOC] (Figure S6).

DIC production is lower than oxygen consumption in all samples, which indicates that DOM consumes O_2 without undergoing complete mineralization. The ratio of O_2 consumption to DIC production ranges from 2 to 11 (Figure S7d), demonstrating that partial photooxidation is the dominant pathway of photolytic processing (i.e., assuming that a 1:1 molar ratio of O_2 consumption to DIC production is indicative of complete photooxidation).[4,9] Ratios of <1 to ∼2 have been reported for terrestrially derived arctic DOM[4,8,9] and up to ∼6.6 for black carbon.[12] High values observed in two oligotrophic samples are attributable to their low DIC yields. The extent of partial oxidation in DOM from temperate regions or in microbially derived DOM using dissolved gas measurements has not been reported previously.

Quantum yields for O_2 consumption and DIC production vary with the DOM source. The isolates, dystrophic lakes, and mesotrophic lake have the lowest oxygen quantum yields (0.32 to 0.52 mmol-O_2/mol-photons), while eutrophic (0.52 to 1.70 mmol-O_2/mol-photons) and oligotrophic waters (0.26 to 1.85 mmol-O_2/mol-photons) have higher values (Figure S7b and Table S9). Similar trends are observed for Φ_{DIC} (Figure S7c), which ranges from 0.09 to 0.11 mmol-DIC/mol-photons in the isolates, dystrophic lakes, and mesotrophic DOM, 0.11 to 0.26 mmol-DIC/mol-photons in eutrophic DOM, and 0.09 to 0.21 mmol-DIC/mol-photons in oligotrophic DOM. Similar Φ_{O2} values of 0.30 to 0.38 mmol-O_2/mol-photons in SRNOM at 369 nm[77] (0.32 in our study), 0.63 to 1.44 mmol-O_2/mol-photons in the Everglades (300−400 nm),[78] and up to 3.77 mmol-O_2/mol-photons in the Gulf of Maine (300−400 nm)[78] have been reported. CO_2 quantum yields in the literature range from ∼1 to >5 mmol-CO_2/mol-photon in the Arctic (350 nm)[4] and from 0.05 to 0.61 in lake samples (300−400 nm).[10]

Significant positive relationships are observed between dissolved gas concentrations and rates of light absorbance (Figure S6), highlighting the importance of [DOC] and light-absorbing DOM in photooxidation. Interestingly, the samples that consume the most O_2 and produce the most DIC (i.e., dystrophic lakes and G3) have low quantum yields. While these three samples have high rates of light absorption due to their high [DOC] (Table S5), they are less efficient in terms of complete and partial photooxidation, suggesting that the underlying DOM composition influences its susceptibility to partial and complete photooxidation.

Role of DOM Composition in Partial Photooxidation. To investigate how DOM composition influences its ability to consume O_2 and undergo complete photomineralization to CO_2, we first use linear regression analysis to compare gas consumption and production with DOM parameters. The considered bulk parameters are independent of [DOC] because they are either normalized to [DOC] (e.g., $SUVA_{254}$) or are ratios derived from optical measurements (e.g., E_2:E_3). Similarly, FT-ICR MS weighted averages are normalized to relative formula intensity. Therefore, this approach allows us to assess how DOM composition impacts quantum yields, which are normalized to the rate of light absorbance, and carbon-normalized gas concentrations across this diverse set of DOM samples.

Φ_{O2} is positively correlated with E_2:E_3, BIX, and H:C_w and negatively correlated with $SUVA_{254}$, DBE_w, and carbon-normalized double bond equivalents (DBE_w/C; $p < 0.05$; Figure S8). Similarly, Φ_{DIC} is positively correlated with E_2:E_3 and FI (Figure S9). Φ_{DIC} trends with BIX, H:C_w, $SUVA_{254}$, EDC, DBE_w, and DBE_w/C are similar to Φ_{O2} trends but are not significant. These trends indicate that the DOM that is lower in MW, highly saturated, and more reduced (i.e., microbially derived and/or highly processed) is more efficient at consuming O_2 and producing DIC. A previous study found positive correlations between Φ_{CO2} and $SUVA_{254}$ using DOM from 25 lakes,[10] which is the opposite of the insignificant negative trend observed here. Interestingly, carbon-normalized DIC production has many of the opposite trends, displaying positive correlations with $SUVA_{254}$, EDC, DBE, and DBE:C and negative trends with E_2:E_3, H:C_w, and BIX. This suggests that more aromatic compounds are associated with DIC production. Carbon-normalized O_2 consumption had no significant relationships.

Spearman rank analysis using FT-ICR MS data demonstrates that unique pools of DOM formulas are associated with O_2 consumption and DIC production. This analysis relates the relative intensity of common individual molecular formulas (1409 formulas in 17 samples) to parameters associated with photooxidation (Section S6). As with linear regression analysis, this comparison includes parameters that are independent of [DOC] (i.e., carbon-normalized gas concentrations and quantum yields) because FT-ICR MS data are based on relative intensity.

Formulas associated with carbon-normalized DIC production and oxygen consumption are in the portion of the van Krevelen diagram typically associated with lignin- and tannin-like formulas[79] (i.e., low H:C; Figure 1b,c). These same formulas are also associated with $SUVA_{254}$ and EDC (Figure S11), indicating that highly aromatic, redox-active formulas are the most likely to react with oxygen and are the most susceptible to decarboxylation. Previous studies indicate that the most photolabile formulas identified using FT-ICR MS are similarly highly aromatic.[9,36,37] This group of formulas are also associated with reactions with oxidants like chorine,[56,80] reactive chlorine species,[56,80] ozone,[42] and hydroxyl radical.[42] Collectively, this analysis demonstrates that electron-rich, aromatic formulas are the most susceptible to photooxidation.

Formulas associated with Φ_{O2} and Φ_{DIC} (Figure 1e,f) are much more highly saturated and more reduced than formulas associated with carbon-normalized gas measurements. As observed with carbon-normalized gas concentrations, both quantum yields are positively correlated with each other (Figure S12). Similar highly saturated formulas are also

https://doi.org/10.1021/acs.est.3c01500
Environ. Sci. Technol. 2023, 57, 11876−11885

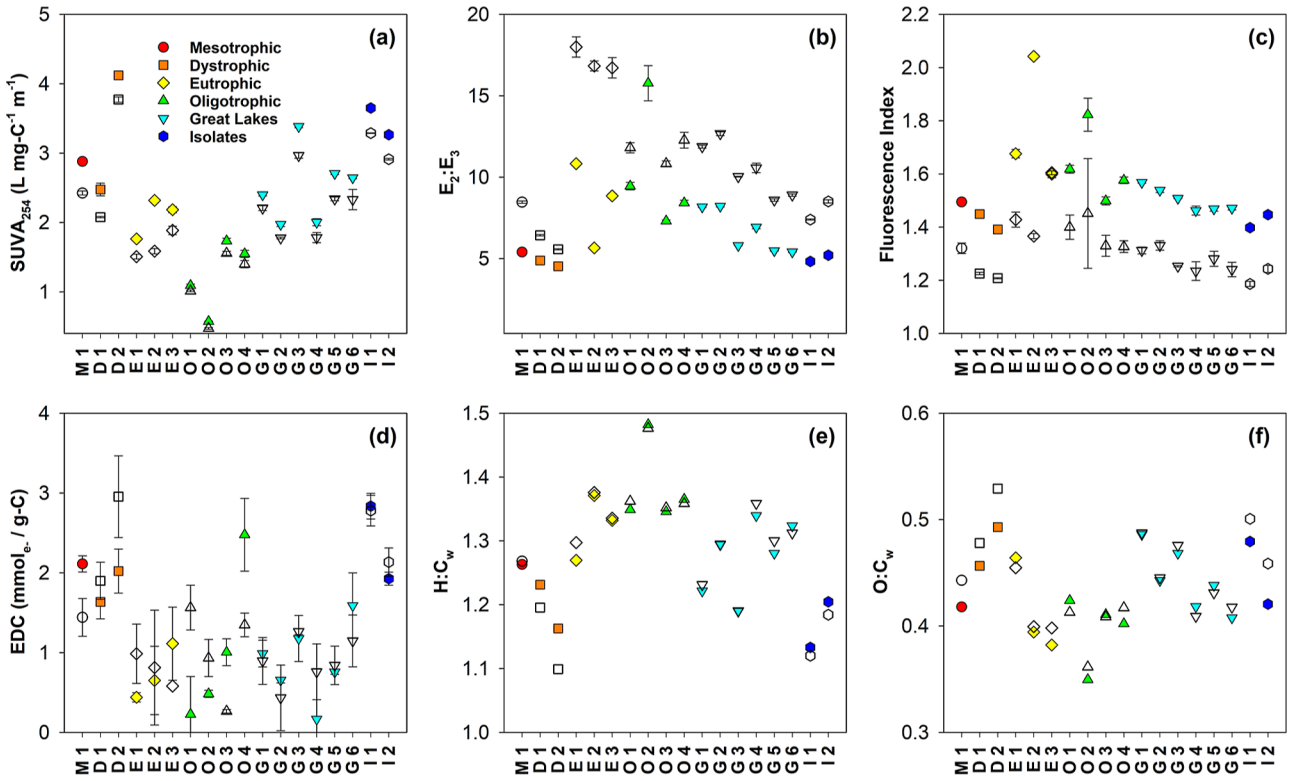

Figure 2. (a) Specific UV absorbance ($SUVA_{254}$), (b) E_2:E_3, (c) fluorescence index, (d) EDC, (e) H:C_w, and (f) O:C_w before (filled) and after (hollow) photooxidation of DOM for 22 h. Error bars are present for all samples except H:C_w and O:C_w and correspond to the standard deviation of triplicate measurements.

associated with singlet oxygen ($^1O_2$) and triplet state DOM (^{3}DOM) quantum yields,[54,61,81] which are photochemically produced reactive intermediates (PPRI) that contribute to indirect contaminant photolysis and likely to DOM partial photooxidation.[8,82,83]

The deviation between formulas associated with carbon-normalized gas concentrations and quantum yields is attributable to several factors. Highly aromatic formulas absorb more light and are more susceptible to oxidation because they are electron-rich.[84] However, on a per photon basis, saturated formulas are more efficient at consuming O_2 and producing DIC. Previous work has shown that high MW, aromatic DOM (i.e., formulas associated with carbon-normalized gas concentrations; Figure 1b,c) is able to quench ^{3}DOM efficiently.[54] Similarly, these highly aromatic compounds can act as antioxidants,[9,54] leading to negative correlations between $SUVA_{254}$ and quantum yields and positive correlations with highly saturated formulas (Figure S8). Therefore, highly aromatic formulas absorb light efficiently and also quench reactive species that are likely to be involved in DOM photooxidation. As a result, Φ_{O2} and Φ_{DIC} are associated with more saturated DOM at the molecular level.

Changes in DOM Bulk Composition after Photolysis. It is important to understand how DOM composition changes during photooxidation because this impacts its subsequent reactivity. For example, DOM can become either more or less bioavailable after photooxidation.[12,14,16,18,20,21] This variable behavior suggests that photooxidation may change DOM composition in different ways,[4,9,10,12,37] which we hypothesize is attributable to initial DOM composition.

To investigate how DOM composition changes during photolysis, we first quantify changes in bulk parameters. Most samples decrease in [DOC] or have [DOC] changes below the LOD during photolysis (Figure S7a), in agreement with previous studies[14,29−31,35,50,85] and with the low DIC yields in this study (Figure 1d). E_2:E_3 increases and $SUVA_{254}$ decreases in all samples (Figure 2a,b and Table S5), indicating that lower MW, aliphatic molecules are produced[14−17] or that higher MW aromatic compounds are photodegraded. While some studies show little or no change in E_2:E_3 or the spectral slope,[57] most studies show increases in these parameters[4,9,29−31,33−35,50,85] and highlight the photolability of aromatic DOM.[30,31,50]

FI and HIX decrease in all but two samples and BIX increases in all samples after irradiation (Figures 2c and S5 and Table S7). Decreases in HIX and increases in BIX are expected as a result of photooxidation.[50] While the decrease in FI is unexpected because low FI values indicate less highly processed DOM, similar decreases in FI have been observed.[50] However, changes in fluorescence indices should be interpreted carefully given the narrowband light source used in this study.[86] Nonetheless, this contradictory result suggests that photooxidation can complicate the interpretation of fluorescence indices for determining the DOM origin.

EDC decreases in nine samples and increases in nine samples (Figure 2d). Decreasing EDC is consistent with the loss of aromatic compounds (i.e., decreasing $SUVA_{254}$; Figure 2a) and with past observations during photolysis of wastewater and DOM isolates.[31,87] In contrast, the increases in EDC observed in this study may be due to the formation of phenols or polyphenols during photooxidation[43,88,89] (e.g., via OH addition to aromatic rings due to the reaction with hydroxyl radical). As discussed below, variable changes in EDC are likely attributable to the initial DOM composition.

https://doi.org/10.1021/acs.est.3c01500
Environ. Sci. Technol. 2023, 57, 11876−11885

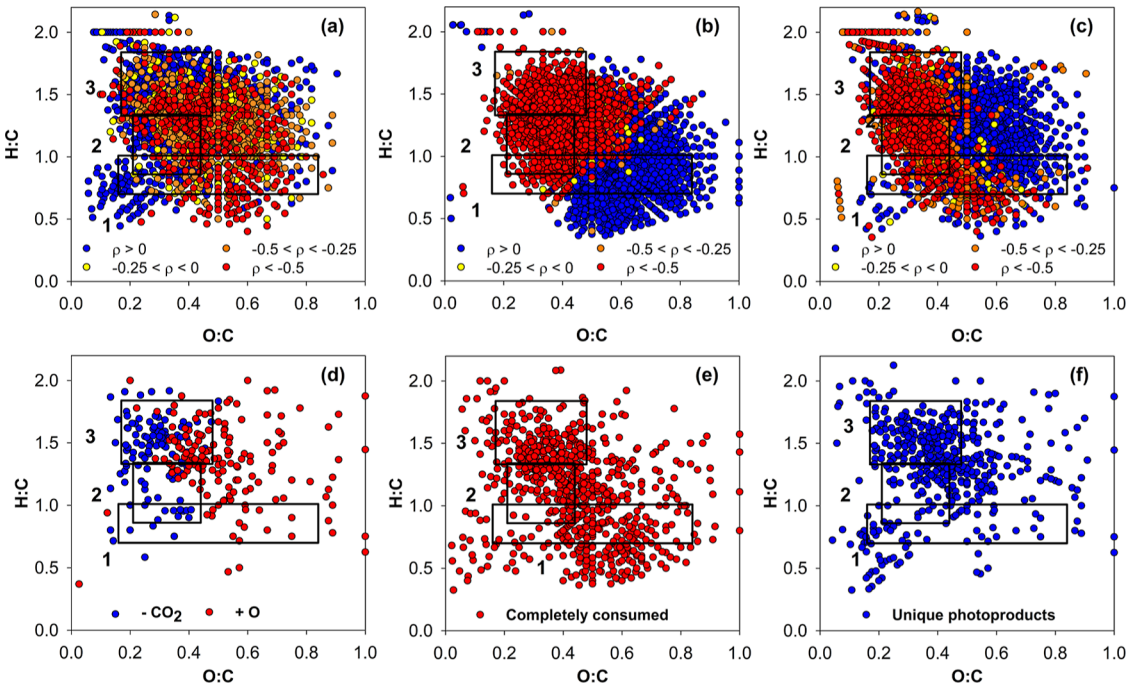

Figure 3. Spearman rank correlations between irradiation time (0, 2, 6, and 24 h) and common formulas in (a) oligotrophic Big Muskellunge Lake (O1), (b) dystrophic Trout Bog (D2), and (c) mesotrophic Allequash Lake (M1). Formulas were required to be present in all four timepoints. Formulas in yellow, orange, and red show formulas that are negatively correlated with increasing light exposure time (i.e., formulas decrease in relative intensity over time). Formulas in blue show formulas that are positively correlated with increasing light exposure time (i.e., formulas increase in relative intensity). (d) Formulas associated with the loss of CO_2 (blue) and the addition of oxygen (red) during photooxidation of eutrophic Lake Mendota (E1). (e) Formulas present only before photooxidation and (f) formulas present only after photooxidation in Lake Mendota (E1). Analogous figures for the remaining lakes are presented in Figures S13−S24. Boxes correspond to (1) lignin-, (2) tannin-, and (3) protein-like regions.[79]

Changes in DOM Molecular Composition after Photolysis. As observed with EDC, variable changes in DOM composition after photolysis are observed at the molecular level. Note that this analysis only considers formulas that are extracted via SPE and that are ionized via negative mode electrospray ionization. Four samples decrease in $H:C_w$, three samples increase in $H:C_w$, and 11 samples have no change. In terms of $O:C_w$, four samples decrease, 11 increase, and three do not change during photooxidation (Figure 2e,f). In general, the samples that decrease in $O:C_w$ also increase in $H:C_w$. Overall, previous studies show that $H:C_w$ typically increases during photolysis,[9,12,22,32,34,36−38] and $O:C_w$ either increases[34,36,38,90] or decreases[9,32,91] during photolysis, although most of these studies only include a small number of samples. The decreases in $H:C_w$ in some samples may be attributable to the degradation of highly saturated formulas associated with Φ_{DIC} and Φ_{O2} (Figure 1e,f). The increase in $O:C_w$ may be due to extensive partial photooxidation, which could incorporate oxygen into DOM molecules during the photooxidation process.

At the individual formula level, there are five possible outcomes after photolysis. Formulas that decrease in relative intensity are considered to be photodegraded, whereas formulas that increase in relative intensity are considered to be photoproduced. Additionally, formulas may be only present in the initial sample ("completely consumed") or only present after photoirradiation ("unique photoproducts"). Finally, formulas with no change in relative intensity are considered to be inert.

We first consider photoproduced and photodegraded formulas in six samples that were irradiated for three different timepoints (Table S10), which allows us to conduct Spearman rank analysis using time as the independent variable (Section S6). The photodegraded formulas in mesotrophic DOM, Lake Michigan, and SRNOM (negative rho values; samples M1, G3, and I1; Figures 3c and S13b,c) are reduced and/or aromatic, whereas photoproduced formulas are oxidized and highly saturated. Thus, photooxidation of these three samples produces DOM that is more oxidized and aliphatic. The photodegraded formulas are similar to the formulas associated with O_2 consumption, DIC production, $SUVA_{254}$, and EDC (Figures 1b,c, and S11).

Different trends are observed in the dystrophic, oligotrophic, and eutrophic lake DOM. DOM from D2 becomes more oxidized (i.e., similar to M1) and more aromatic following photolysis (Figure 3b). We hypothesize that the phenolic and aromatic compounds in this sample act as quenchers for reactive species and/or react with PPRI to form more aromatic compounds. In contrast, DOM from O1 and E1 becomes more reduced and more aliphatic (Figures 3a and S13a), which is the opposite to the molecular trends observed in M1, G3, and I1. DOM from the oligotrophic and eutrophic lakes is highly processed due to a long hydraulic residence time (Table S2) and eutrophic nature, respectively.[3] Therefore, it is likely that the most highly reactive formulas have already been removed via photolytic or biological processing. The reduced nature of photoproducts is similar to that in previous studies in the Arctic[9,39] and to that of photooxidized marine DOM.[32]

DOM composition changes in the remaining 12 samples follow one of these three patterns or exhibit little to no change (Figures S14 and S15). These samples were irradiated for one timepoint and assessed based on ≥10% changes in relative

https://doi.org/10.1021/acs.est.3c01500
Environ. Sci. Technol. 2023, 57, 11876−11885

intensity before and after light exposure (t_0 vs t_{24}; Section S6 and Figure S4). As observed for M1, G3, and I1, DOM from G1, E3, and O4 become more highly saturated and more oxidized following photolysis (Figures S14f and S15i,g). D1 and I2 DOM become more aromatic and more oxidized (Figures S14c and S15h), as observed for D2. G2 behaves similarly to E1 and O1, forming DOM that is more highly saturated and reduced (Figure S14g). There is an overlap between photodegraded and photoproduced formulas in the remaining samples (O2, E2, O3, G4, G5, and G6); these samples also had small changes in weighted averages and gas concentrations (Figures 1a,d and 2e,f) and therefore undergo minimal changes during photooxidation. Overall, despite previous studies suggesting that DOM should become more oxidized[34,36,38,90] and more aliphatic,[9,12,22,32,34,36−38] we show that overall changes in weighted averages and in common individual formulas are highly variable.

Despite the differences observed in formulas present both before and after irradiation, completely consumed formulas and unique photoproducts are similar across all samples. We identify 351 ± 71 completely consumed formulas and 309 ± 77 photoproducts (Figures 3e,f and S16−S21 and Table S12). The photoproducts are generally more oxidized and more saturated than the consumed formulas, with O:C_w and H:C_w of the unique formulas increasing by 6.7 ± 23.2 and 2.7 ± 11.7%, respectively, on average. While deviations from this trend are observed in a few samples with very small changes in DOM composition, these results are consistent with the hypothesis that photooxidation generates DOM that is more oxidized and aliphatic in nature even though overall changes in DOM produce opposite trends in many waters.

There is molecular level evidence for partial photooxidation via oxygen addition in all samples. Photoproduct formulas that are attributable to the addition of a single oxygen atom are identified by comparing unique photoproducts with the initial DOM formula assignment mass list (Section S6). As observed in studies using ^{18}O labeling to observe oxygen addition,[8,18] these photoproducts are tightly clustered at O:C > 0.4 (Figures S22−S24). The number of oxygenated photoproducts ranges from 113 in O1 to 288 in D1 (Table S12). Therefore, partial photooxidation occurs in all samples, regardless of the amount of oxygen consumption or changes in O:C_w. For example, O2 and G2 do not have significant oxygen consumption, yet have 128 and 175 oxygenated formulas, respectively. Similarly, G5 has 119 oxygenated formulas despite a decrease in O:C_w.

Loss of CO_2 at the molecular level similarly provides evidence of complete photooxidation. The number of decarboxylated formulas ranges from 39 in D2 to 147 in G2 (Figures S22−S24 and Table S12). As observed with oxygen addition, the number of decarboxylated formulas does not correlate with measured DIC production. However, a lower number of decarboxylated formulas than that of oxygenated photoproducts is consistent with lower DIC production compared to oxygen consumption (Figure 1a,d). Additionally, these highly saturated and reduced formulas are similar to the formulas associated with decarboxylation of DOM due to the reaction with hydroxyl radical,[42] suggesting that PPRI such as hydroxyl radicals may contribute to photodecarboxylation. While outside the scope of this study, more work is needed to identify specific PPRI and the role that they play in this process.

ENVIRONMENTAL IMPLICATIONS

DOM from a wide variety of temperate lakes, including nearshore samples from two Great Lakes, is susceptible to extensive partial photooxidation. Importantly, there is evidence of oxidation and photodecarboxylation at the molecular level in all cases (Figures 3d and S22−S24), regardless of the amount of oxygen consumption, DIC production, or the change in O:C_w during photooxidation. Within these waters, aromatic formulas are the primary drivers of DIC production and O_2 consumption (Figure 1b,c); these same formulas are generally consumed during photooxidation. In contrast, high O_2 and DIC quantum yields are associated with saturated formulas (Figure 1e,f), as observed for quantum yields of $^1O_2$ and ^{3}DOM.[54,61]

The molecular composition of DOM determines its susceptibility to partial photooxidation. More aromatic and terrestrial DOM (e.g., from dystrophic lakes and G3) have lower ratios of oxygen consumption to DIC production (Figure S7d), indicating that it is more susceptible to complete photooxidation. More highly processed waters (e.g., eutrophic, oligotrophic, and Great Lakes DOM) are dominated by partial photooxidation and will produce less DIC. These findings have important implications for understanding and potentially predicting the extent of CO_2 production in inland waters. Overall, this variability reflects previous observations of terrestrially derived DOM being more susceptible to photooxidation and more likely to undergo complete mineralization, whereas more "processed" DOM has already undergone extensive reactions in the environment and is less reactive with sunlight.[4]

The change in DOM composition following partial photooxidation is also influenced by its composition. Many of the lakes with highly aromatic DOM become more aliphatic and more oxidized, which is the expected change in DOM composition following photooxidation. However, other highly aromatic DOM from waters with heavy input from wetlands (D2, D1, and I2) become more aromatic and more oxidized, while waters with DOM that is more highly processed or more microbial in nature, such as many of the eutrophic and oligotrophic lakes of the NTL-LTER network, become more reduced and more aliphatic or have very minimal changes in composition at the molecular level. The wide variety in changes in DOM composition in this study helps explain the variable trends in bioavailability of DOM following photooxidation.[14,16,19−25,27,28,92,93]

ASSOCIATED CONTENT

Supporting Information

The Supporting Information is available free of charge at https://pubs.acs.org/doi/10.1021/acs.est.3c01500.

Additional experimental details, sample information and characterization, dissolved gas kinetics experiments, linear regression analysis, and FT-ICR MS analysis information (PDF)

AUTHOR INFORMATION

Corresponding Author

Christina K. Remucal − *Environmental Chemistry and Technology Program and Department of Civil and Environmental Engineering, University of Wisconsin-Madison, Madison, Wisconsin 53706, United States;* orcid.org/

https://doi.org/10.1021/acs.est.3c01500
Environ. Sci. Technol. 2023, 57, 11876−11885

0000-0003-4285-7638; Phone: (608) 262-1820; Email: remucal@wisc.edu; Fax: (608) 262-0454

Authors

Reid P. Milstead − *Environmental Chemistry and Technology Program, University of Wisconsin-Madison, Madison, Wisconsin 53706, United States;* orcid.org/0000-0002-9382-6703

Emma R. Horvath − *Department of Civil and Environmental Engineering, University of Wisconsin-Madison, Madison, Wisconsin 53706, United States*

Complete contact information is available at: https://pubs.acs.org/10.1021/acs.est.3c01500

Notes

The authors declare no competing financial interest.

■ ACKNOWLEDGMENTS

This project was supported by the National Science Foundation (EAR-2104716) and an Anna Grant Birge Memorial Award. We acknowledge Noah Lottig, Alice Ogden-Nussbaum, and Ted Bier from the University of Wisconsin-Madison Trout Lake Research Station and the Hasler Laboratory of Limnology for facilitating sample collection through the support of the NTL-LTER program (NSF DEB-2025982). We acknowledge the UW-Madison Human Proteomics Program Mass Spectrometry Facility for support in obtaining mass spectrometry data, Yanlong Zhu for assistance with instrument operation, and NIH S10OD018475 for acquisition of the high-resolution mass spectrometer.

■ REFERENCES

(1) Battin, T. J.; Luyssaert, S.; Kaplan, L. A.; Aufdenkampe, A. K.; Richter, A.; Tranvik, L. J. The boundless carbon cycle. *Nat. Geosci.* **2009**, *2*, 598−600.

(2) Buffam, I.; Turner, M. G.; Desai, A. R.; Hanson, P. C.; Rusak, J. A.; Lottig, N. R.; Stanley, E. H.; Carpenter, S. R. Integrating aquatic and terrestrial components to construct a complete carbon budget for a north temperate lake district. *Glob. Change Biol.* **2011**, *17*, 1193−1211.

(3) Hanson, P. C.; Buffam, I.; Rusak, J. A.; Stanley, E. H.; Watras, C. Quantifying lake allochthonous organic carbon budgets using a simple equilibrium model. *Limnol. Oceanogr.* **2014**, *59*, 167−181.

(4) Cory, R. M.; Ward, C. P.; Crump, B. C.; Kling, G. W. Sunlight controls water column processing of carbon in arctic fresh waters. *Science* **2014**, *345*, 925−928.

(5) Cole, J. J.; Caraco, N. F.; Kling, G. W.; Kratz, T. K. Carbon dioxide supersaturation in the surface waters of lakes. *Science* **1994**, *265*, 1568−1570.

(6) Raymond, P. A.; Hartmann, J.; Lauerwald, R.; Sobek, S.; McDonald, C.; Hoover, M.; Butman, D.; Striegl, R.; Mayorga, E.; Humborg, C.; Kortelainen, P.; Dürr, H.; Meybeck, M.; Ciais, P.; Guth, P. Global carbon dioxide emissions from inland waters. *Nature* **2013**, *503*, 355−359.

(7) Global Carbon Project (GCP). https://www.globalcarbonproject.org/carbonbudget/21/publications.html (accessed on Aug 08, 2022).

(8) Ward, C. P.; Cory, R. M. Assessing the prevalence, products, and pathways of dissolved organic matter partial photo-oxidation in arctic surface waters. *Environ. Sci. Process. Impacts* **2020**, *22*, 1214−1223.

(9) Ward, C. P.; Cory, R. M. Complete and partial photo-oxidation of dissolved organic matter draining permafrost soils. *Environ. Sci. Technol.* **2016**, *50*, 3545−3553.

(10) Koehler, B.; Broman, E.; Tranvik, L. J. Apparent quantum yield of photochemical dissolved organic carbon mineralization in lakes. *Limnol. Oceanogr.* **2016**, *61*, 2207−2221.

(11) Hanson, P. C.; Hamilton, D. P.; Stanley, E. H.; Preston, N.; Langman, O. C.; Kara, E. L. Fate of allochthonous dissolved organic carbon in lakes: A quantitative approach. *PLoS One* **2011**, *6*, No. e21884.

(12) Ward, C. P.; Sleighter, R. L.; Hatcher, P. G.; Cory, R. M. Insights into the complete and partial photooxidation of black carbon in surface waters. *Environ. Sci. Process. Impacts* **2014**, *16*, 721−731.

(13) Waggoner, D. C.; Wozniak, A. S.; Cory, R. M.; Hatcher, P. G. The role of reactive oxygen species in the degradation of lignin derived dissolved organic matter. *Geochim. Cosmochim. Acta* **2017**, *208*, 171−184.

(14) Wetzel, R. G.; Hatcher, P. G.; Bianchi, T. S. Natural photolysis by ultraviolet irradiance of recalcitrant dissolved organic matter to simple substrates for rapidbacterial metabolism. *Limnol. Oceanogr.* **1995**, *40*, 1369−1380.

(15) Kieber, D. J.; McDaniel, J.; Mopper, K. Photochemical source of biological substrates in sea water: implications for carbon cycling. *Nature* **1989**, *341*, 637−639.

(16) Pullin, M. J.; Bertilsson, S.; Goldstone, J. V.; Voelker, B. M. Effects of sunlight and hydroxyl radical on dissolved organic matter: bacterial growth efficiency and production of carboxylic acids and other substrates. *Limnol. Oceanogr.* **2004**, *49*, 2011−2022.

(17) Mopper, K.; Zhou, X.; Kieber, R. J.; Kieber, D. J.; Sikorski, R. J.; Jones, R. D. Photochemical degradation of dissolved organic carbon and its impact on the oceanic carbon cycle. *Nature* **1991**, *353*, 60−62.

(18) Cory, R. M.; McNeill, K.; Cotner, J. P.; Amado, A.; Purcell, J. M.; Marshall, A. G. Singlet oxygen in the coupled photochemical and biochemical oxidation of dissolved organic matter. *Environ. Sci. Technol.* **2010**, *44*, 3683−3689.

(19) Sleighter, R. L.; Cory, R. M.; Kaplan, L. A.; Abdulla, H. A. N.; Hatcher, P. G. A coupled geochemical and biogeochemical approach to characterize the bioreactivity of dissolved organic matter from a headwater stream: biogeochemistry and lability of stream DOM. *J. Geophys. Res.: Biogeosci.* **2014**, *119*, 1520−1537.

(20) Tranvik, L.; Kokalj, S. Decreased biodegradability of algal DOC due to interactive effects of UV radiation and humic matter. *Aquat. Microb. Ecol.* **1998**, *14*, 301−307.

(21) Moran, M. A.; Zepp, R. G. Role of photoreactions in the formation of biologically labile compounds from dissolved organic matter. *Limnol. Oceanogr.* **1997**, *42*, 1307−1316.

(22) Ward, C. P.; Nalven, S. G.; Crump, B. C.; Kling, G. W.; Cory, R. M. Photochemical alteration of organic carbon draining permafrost soils shifts microbial metabolic pathways and stimulates respiration. *Nat. Commun.* **2017**, *8*, 772.

(23) Benner, R.; Biddanda, B. Photochemical transformations of surface and deep marine dissolved organic matter: effects on bacterial growth. *Limnol. Oceanogr.* **1998**, *43*, 1373−1378.

(24) Tranvik, L. J.; Bertilsson, S. Contrasting effects of solar UV radiation on dissolved organic sources for bacterial growth. *Ecol. Lett.* **2001**, *4*, 458−463.

(25) Judd, K. E.; Crump, B. C.; Kling, G. W. Bacterial responses in activity and community composition to photo-oxidation of dissolved organic matter from soil and surface waters. *Aquat. Sci.* **2007**, *69*, 96−107.

(26) Cory, R. M.; Crump, B. C.; Dobkowski, J. A.; Kling, G. W. Surface exposure to sunlight stimulates CO_2 release from permafrost soil carbon in the arctic. *Proc. Natl. Acad. Sci. U.S.A.* **2013**, *110*, 3429−3434.

(27) Biddanda, B. A.; Cotner, J. B. Enhancement of dissolved organic matter bioavailability by sunlight and its role in the carbon cycle of lakes Superior and Michigan. *J. Gt. Lakes Res.* **2003**, *29*, 228−241.

(28) Cory, R. M.; Kling, G. W. Interactions between sunlight and microorganisms influence dissolved organic matter degradation along the aquatic continuum. *Limnol. Oceanogr. Lett.* **2018**, *3*, 102−116.

(29) Helms, J. R.; Stubbins, A.; Ritchie, J. D.; Minor, E. C.; Kieber, D. J.; Mopper, K. Absorption spectral slopes and slope ratios as indicators of molecular weight, source, and photobleaching of

chromophoric dissolved organic matter. *Limnol. Oceanogr.* **2008**, *53*, 955−969.
(30) Mann, P. J.; Davydova, A.; Zimov, N.; Spencer, R. G. M.; Davydov, S.; Bulygina, E.; Zimov, S.; Holmes, R. M. Controls on the composition and lability of dissolved organic matter in Siberia's Kolyma River Basin. *J. Geophys. Res.: Biogeosci.* **2012**, *117*, G01028.
(31) Sharpless, C. M.; Aeschbacher, M.; Page, S. E.; Wenk, J.; Sander, M.; McNeill, K. Photooxidation-induced changes in optical, electrochemical, and photochemical properties of humic substances. *Environ. Sci. Technol.* **2014**, *48*, 2688−2696.
(32) Gonsior, M.; Hertkorn, N.; Conte, M. H.; Cooper, W. J.; Bastviken, D.; Druffel, E.; Schmitt-Kopplin, P. Photochemical production of polyols arising from significant photo-transformation of dissolved organic matter in the oligotrophic surface ocean. *Mar. Chem.* **2014**, *163*, 10−18.
(33) Lou, T.; Xie, H. Photochemical alteration of the molecular weight of dissolved organic matter. *Chemosphere* **2006**, *65*, 2333−2342.
(34) Gonsior, M.; Schmitt-Kopplin, P.; Bastviken, D. Depth-dependent molecular composition and photo-reactivity of dissolved organic matter in a boreal lake under winter and summer conditions. *Biogeosciences* **2013**, *10*, 6945−6956.
(35) Spencer, R. G. M.; Stubbins, A.; Hernes, P. J.; Baker, A.; Mopper, K.; Aufdenkampe, A. K.; Dyda, R. Y.; Mwamba, V. L.; Mangangu, A. M.; Wabakanghanzi, J. N.; Six, J. Photochemical degradation of dissolved organic matter and dissolved lignin phenols from the Congo River. *J. Geophys. Res. Biogeosci.* **2009**, *114*, G03010.
(36) Gonsior, M.; Peake, B. M.; Cooper, W. T.; Podgorski, D.; D'Andrilli, J.; Cooper, W. J. Photochemically induced changes in dissolved organic matter identified by ultrahigh resolution Fourier transform ion cyclotron resonance mass spectrometry. *Environ. Sci. Technol.* **2009**, *43*, 698−703.
(37) Stubbins, A.; Spencer, R. G. M.; Chen, H.; Hatcher, P. G.; Mopper, K.; Hernes, P. J.; Mwamba, V. L.; Mangangu, A. M.; Wabakanghanzi, J. N.; Six, J. Illuminated darkness: molecular signatures of Congo River dissolved organic matter and its photochemical alteration as revealed by ultrahigh precision mass spectrometry. *Limnol. Oceanogr.* **2010**, *55*, 1467−1477.
(38) Schmitt-Kopplin, P.; Hertkorn, N.; Schulten, H.-R.; Kettrup, A. Structural changes in a dissolved soil humic acid during photochemical degradation processes under O_2 and N_2 atmosphere. *Environ. Sci. Technol.* **1998**, *32*, 2531−2541.
(39) Bowen, J. C.; Ward, C. P.; Kling, G. W.; Cory, R. M. Arctic amplification of global warming strengthened by sunlight oxidation of permafrost carbon to CO_2. *Geophys. Res. Lett.* **2020**, *47*, No. e2020GL087085.
(40) North Temperate Lakes US Long-Term Ecological Research Network. https://lter.limnology.wisc.edu/ (accessed on Feb 09, 2022).
(41) Weishaar, J. L.; Aiken, G. R.; Bergamaschi, B. A.; Fram, M. S.; Fujii, R.; Mopper, K. Evaluation of specific ultraviolet absorbance as an indicator of the chemical composition and reactivity of dissolved organic carbon. *Environ. Sci. Technol.* **2003**, *37*, 4702−4708.
(42) Remucal, C. K.; Salhi, E.; Walpen, N.; von Gunten, U. Molecular-level transformation of dissolved organic matter during oxidation by ozone and hydroxyl radical. *Environ. Sci. Technol.* **2020**, *54*, 10351−10360.
(43) Walpen, N.; Getzinger, G. J.; Schroth, M. H.; Sander, M. Electron-donating phenolic and electron-accepting quinone moieties in peat dissolved organic matter: quantities and redox transformations in the context of peat biogeochemistry. *Environ. Sci. Technol.* **2018**, *52*, 5236−5245.
(44) Walpen, N.; Houska, J.; Salhi, E.; Sander, M.; von Gunten, U. Quantification of the electron donating capacity and UV absorbance of dissolved organic matter during ozonation of secondary wastewater effluent by an assay and an automated analyzer. *Water Res.* **2020**, *185*, 116235.
(45) McKnight, D. M.; Boyer, E. W.; Westerhoff, P. K.; Doran, P. T.; Kulbe, T.; Andersen, D. T. Spectrofluorometric characterization of dissolved organic matter for indication of precursor organic material and aromaticity. *Limnol. Oceanogr.* **2001**, *46*, 38−48.
(46) Ohno, T. Fluorescence inner-filtering correction for determining the humification index of dissolved organic matter. *Environ. Sci. Technol.* **2002**, *36*, 742−746.
(47) Huguet, A.; Vacher, L.; Relexans, S.; Saubusse, S.; Froidefond, J. M.; Parlanti, E. Properties of fluorescent dissolved organic matter in the Gironde Estuary. *Org. Geochem.* **2009**, *40*, 706−719.
(48) Bulman, D. M.; Mezyk, S. P.; Remucal, C. K. The impact of pH and irradiation wavelength on the production of reactive oxidants during chlorine photolysis. *Environ. Sci. Technol.* **2019**, *53*, 4450−4459.
(49) Remucal, C. K.; McNeill, K. Photosensitized amino acid degradation in the presence of riboflavin and its derivatives. *Environ. Sci. Technol.* **2011**, *45*, 5230−5237.
(50) Hansen, A. M.; Kraus, T. E. C.; Pellerin, B. A.; Fleck, J. A.; Downing, B. D.; Bergamaschi, B. A. Optical properties of dissolved organic matter (DOM): Effects of biological and photolytic degradation. *Limnol. Oceanogr.* **2016**, *61*, 1015−1032.
(51) Vähätalo, A. V.; Salkinoja -Salonen, M.; Taalas, P.; Salonen, K. Spectrum of the quantum yield for photochemical mineralization of dissolved organic carbon in a humic lake. *Limnol. Oceanogr.* **2000**, *45*, 664−676.
(52) Koehler, B.; Powers, L. C.; Cory, R. M.; Einarsdóttir, K.; Gu, Y.; Tranvik, L. J.; Vähätalo, A. V.; Ward, C. P.; Miller, W. L. Interlaboratory differences in the apparent quantum yield for the photochemical production of dissolved inorganic carbon in inland waters and implications for photochemical rate modeling. *Limnol. Oceanogr. Methods* **2022**, *20*, 320−337.
(53) Laszakovits, J. R.; Berg, S. M.; Anderson, B. G.; O'Brien, J. E.; Wammer, K. H.; Sharpless, C. M. *p*-Nitroanisole/pyridine and *p*-nitroacetophenone/pyridine actinometers revisited: quantum yield in comparison to ferrioxalate. *Environ. Sci. Technol. Lett.* **2017**, *4*, 11−14.
(54) Maizel, A. C.; Remucal, C. K. Molecular composition and photochemical reactivity of size-fractionated dissolved organic matter. *Environ. Sci. Technol.* **2017**, *51*, 2113−2123.
(55) Dittmar, T.; Koch, B.; Hertkorn, N.; Kattner, G. A simple and efficient method for the solid-phase extraction of dissolved organic matter (SPE-DOM) from seawater. *Limnol. Oceanogr. Methods* **2008**, *6*, 230−235.
(56) Bulman, D. M.; Remucal, C. K. Role of reactive halogen species in disinfection byproduct formation during chlorine photolysis. *Environ. Sci. Technol.* **2020**, *54*, 9629−9639.
(57) Gonsior, M.; Schmitt-Kopplin, P.; Stavklint, H.; Richardson, S. D.; Hertkorn, N.; Bastviken, D. Changes in dissolved organic matter during the treatment processes of a drinking water plant in Sweden and formation of previously unknown disinfection byproducts. *Environ. Sci. Technol.* **2014**, *48*, 12714−12722.
(58) Ziegler, G.; Gonsior, M.; Fisher, D. J.; Schmitt-Kopplin, P.; Tamburri, M. N. Formation of brominated organic compounds and molecular transformations in dissolved organic matter (DOM) after ballast water treatment with sodium dichloroisocyanurate dihydrate (DICD). *Environ. Sci. Technol.* **2019**, *53*, 8006−8016.
(59) Maizel, A. C.; Li, J.; Remucal, C. K. Relationships between dissolved organic matter composition and photochemistry in lakes of diverse trophic status. *Environ. Sci. Technol.* **2017**, *51*, 9624−9632.
(60) Maizel, A. C.; Remucal, C. K. The effect of advanced secondary municipal wastewater treatment on the molecular composition of dissolved organic matter. *Water Res.* **2017**, *122*, 42−52.
(61) Berg, S. M.; Whiting, Q. T.; Herrli, J. A.; Winkels, R.; Wammer, K. H.; Remucal, C. K. The role of dissolved organic matter composition in determining photochemical reactivity at the molecular level. *Environ. Sci. Technol.* **2019**, *53*, 11725−11734.
(62) Koch, B. P.; Witt, M.; Engbrodt, R.; Dittmar, T.; Kattner, G. Molecular formulae of marine and terrigenous dissolved organic matter detected by electrospray ionization Fourier transform ion cyclotron resonance mass spectrometry. *Geochim. Cosmochim. Acta* **2005**, *69*, 3299−3308.

(63) Minor, E.; Stephens, B. Dissolved organic matter characteristics within the Lake Superior watershed. *Org. Geochem.* **2008**, *39*, 1489−1501.
(64) Mostovaya, A.; Koehler, B.; Guillemette, F.; Brunberg, A.-K.; Tranvik, L. J. Effects of compositional changes on reactivity continuum and decomposition kinetics of lake dissolved organic matter. *J. Geophys. Res. Biogeosci.* **2016**, *121*, 1733−1746.
(65) Önnby, L.; Walpen, N.; Salhi, E.; Sander, M.; von Gunten, U. Two analytical approaches quantifying the electron donating capacities of dissolved organic matter to monitor its oxidation during chlorination and ozonation. *Water Res.* **2018**, *144*, 677−689.
(66) Aeschbacher, M.; Graf, C.; Schwarzenbach, R. P.; Sander, M. Antioxidant properties of humic substances. *Environ. Sci. Technol.* **2012**, *46*, 4916−4925.
(67) Helms, J. R.; Stubbins, A.; Perdue, E. M.; Green, N. W.; Chen, H.; Mopper, K. Photochemical bleaching of oceanic dissolved organic matter and its effect on absorption spectral slope and fluorescence. *Mar. Chem.* **2013**, *155*, 81−91.
(68) Zsolnay, A.; Baigar, E.; Jimenez, M.; Steinweg, B.; Saccomandi, F. Differentiating with fluorescence spectroscopy the sources of dissolved organic matter in soils subjected to drying. *Chemosphere* **1999**, *38*, 45−50.
(69) Fleck, J. A.; Gill, G.; Bergamaschi, B. A.; Kraus, T. E. C.; Downing, B. D.; Alpers, C. N. Concurrent photolytic degradation of aqueous methylmercury and dissolved organic matter. *Sci. Total Environ.* **2014**, *484*, 263−275.
(70) Li, H.; Minor, E. C. Dissolved organic matter in Lake Superior: Insights into the effects of extraction methods on chemical composition. *Environ. Sci. Process. Impacts* **2015**, *17*, 1829−1840.
(71) Minor, E. C.; Oyler, A. R. Dissolved organic matter in large lakes: A key but understudied component of the carbon cycle. *Biogeochemistry* **2021**, *164*, 295−318.
(72) Zigah, P. K.; Minor, E. C.; Werne, J. P. Radiocarbon and stable-isotope geochemistry of organic and inorganic carbon in Lake Superior. *Glob. Biogeochem. Cycles* **2012**, *26*, GB1023.
(73) Biddanda, B. A.; Cotner, J. B. Love Handles in Aquatic Ecosystems: The Role of Dissolved Organic Carbon Drawdown, Resuspended Sediments, and Terrigenous Inputs in the Carbon Balance of Lake Michigan. *Ecosystems* **2002**, *5*, 431−445.
(74) Cotner, J. B.; Johengen, T. H.; Biddanda, B. A. Intense winter heterotrophic production stimulated by benthic resuspension. *Limnol. Oceanogr.* **2000**, *45*, 1672−1676.
(75) Fujimoto, M.; Cavaletto, J.; Liebig, J. R.; McCarthy, A.; Vanderploeg, H. A.; Denef, V. J. Spatiotemporal distribution of bacterioplankton functional groups along a freshwater estuary to pelagic gradient in Lake Michigan. *J. Gt. Lakes Res.* **2016**, *42*, 1036−1048.
(76) Balgooyen, S.; Remucal, C. K. Tributary loading and sediment desorption as sources of PFAS to receiving waters. *ACS ES&T Water* **2022**, *2*, 436−445.
(77) Ward, C. P.; Bowen, J. C.; Freeman, D. H.; Sharpless, C. M. Rapid and reproducible characterization of the wavelength dependence of aquatic photochemical reactions using light-emitting diodes. *Environ. Sci. Technol. Lett.* **2021**, *8*, 437−442.
(78) Andrews, S. S.; Caron, S.; Zafiriou, O. C. Photochemical oxygen consumption in marine waters: a major sink for colored dissolved organic matter? *Limnol. Oceanogr.* **2000**, *45*, 267−277.
(79) Laszakovits, J. R.; MacKay, A. A. Data-based chemical class regions for van Krevelen diagrams. *J. Am. Soc. Mass Spectrom.* **2022**, *33*, 198−202.
(80) Milstead, R. P.; Remucal, C. K. Molecular-level insights into the formation of traditional and novel halogenated disinfection by-products. *ACS ES&T Water* **2021**, *1*, 1966−1974.
(81) Berg, S. M.; Peterson, B. D.; McMahon, K. D.; Remucal, C. K. Spatial and temporal variability of dissolved organic matter molecular composition in a stratified eutrophic lake. *J. Geophys. Res. Biogeosci.* **2022**, *127*, No. e2021JG006550.
(82) Remucal, C. K. The role of indirect photochemical degradation in the environmental fate of pesticides: a review. *Environ. Sci. Process. Impacts* **2014**, *16*, 628−653.
(83) McNeill, K.; Canonica, S. Triplet state dissolved organic matter in aquatic photochemistry: reaction mechanisms, substrate scope, and photophysical properties. *Environ. Sci. Process. Impacts* **2016**, *18*, 1381−1399.
(84) Berg, S. M.; Wammer, K. H.; Remucal, C. K. Dissolved organic matter photoreactivity is determined by its optical properties, redox activity, and molecular composition. *Environ. Sci. Technol.* **2023**, *57*, 6703−6711.
(85) Dalzell, B. J.; Minor, E. C.; Mopper, K. M. Photodegradation of estuarine dissolved organic matter: a multi-method assessment of DOM transformation. *Org. Geochem.* **2009**, *40*, 243−257.
(86) Del Vecchio, R.; Blough, N. V. On the origin of the optical properties of humic substances. *Environ. Sci. Technol.* **2004**, *38*, 3885−3891.
(87) Du, Y.; Wu, Q.-Y.; Lv, X.-T.; Ye, B.; Zhan, X.-M.; Lu, Y.; Hu, H.-Y. Electron donating capacity reduction of dissolved organic matter by solar irradiation reduces the cytotoxicity formation potential during wastewater chlorination. *Water Res.* **2018**, *145*, 94−102.
(88) Hotta, H.; Sakamoto, H.; Nagano, S.; Osakai, T.; Tsujino, Y. Unusually large numbers of electrons for the oxidation of polyphenolic antioxidants. *Biochim. Biophys. Acta* **2001**, *1526*, 159−167.
(89) Hotta, H.; Nagano, S.; Ueda, M.; Tsujino, Y.; Koyama, J.; Osakai, T. Higher radical scavenging activities of polyphenolic antioxidants can be ascribed to chemical reactions following their oxidation. *Biochim. Biophys. Acta* **2002**, *1572*, 123−132.
(90) Herzsprung, P.; Wentzky, V.; Kamjunke, N.; von Tümpling, W.; Wilske, C.; Friese, K.; Boehrer, B.; Reemtsma, T.; Rinke, K.; Lechtenfeld, O. J. Improved Understanding of Dissolved Organic Matter Processing in Freshwater Using Complementary Experimental and Machine Learning Approaches. *Environ. Sci. Technol.* **2020**, *54*, 13556−13565.
(91) Wilske, C.; Herzsprung, P.; Lechtenfeld, O. J.; Kamjunke, N.; von Tümpling, W. Photochemically induced changes of dissolved organic matter in a humic-rich and forested stream. *Water* **2020**, *12*, 331.
(92) Vallino, J. J.; Hopkinson, C. S.; Hobbie, J. E. Modeling bacterial utilization of dissolved organic matter: optimization replaces monod growth kinetics. *Limnol. Oceanogr.* **1996**, *41*, 1591−1609.
(93) Sun, L.; Perdue, E. M.; Meyer, J. L.; Weis, J. Use of elemental composition to predict bioavailability of dissolved organic matter in a Georgia river. *Limnol. Oceanogr.* **1997**, *42*, 714−721.

https://doi.org/10.1021/acs.est.3c01500
Environ. Sci. Technol. 2023, 57, 11876−11885